

# Thermomechanical squeezing below the 3dB limit

A. Szorkovszky,<sup>1</sup> G.A. Brawley,<sup>1</sup> A.C. Doherty,<sup>2</sup> and W.P. Bowen<sup>1,\*</sup>

<sup>1</sup>Centre for Engineered Quantum Systems, University of Queensland, Australia

<sup>2</sup>Centre for Engineered Quantum Systems, University of Sydney, Australia

(Dated: February 25, 2019)

While cooling techniques are commonly used to remove thermal noise in an oscillator, parametric modulation of the oscillator can reduce both thermal and zero-point noise in one quadrature of motion. This “noise squeezing” property has been widely demonstrated, but has found little use in practice due to a well-known 3dB limit to the squeezing in equilibrium. Using a standard AFM cantilever, we experimentally break this limit by combining optimal estimation and detuned parametric amplification. We observe squeezing of the noise by more than 5dB when the parametric modulation is applied. This squeezing—limited only by the oscillator Q-factor—could be used at room temperature to improve the stability and resolution of sensors, as well as in the low temperature regime to achieve mechanical squeezing below the quantum zero-point motion.

High-quality mechanical oscillators are widely used for weak force detection[1, 2], nano-scale control[3, 4] and quantum state engineering[5, 6]. Periodic modulation of the spring constant or effective mass of a harmonic oscillator at twice its resonance frequency  $f_0$  leads to parametric amplification[7], which enables a range of practical applications such as sensing[8] and information storage and processing[9]. In sensing, for example, mechanical oscillations that are in-phase with the drive can be pre-amplified above the measurement noise floor. This is commonly employed in nano-electromechanical systems where measurement noise is generally dominant[8, 10]. Such phase-sensitive amplification is also noiseless, which is useful in a quantum measurement context to observe signals below the standard quantum limit (SQL) on sensitivity[11]. These pre-amplified signals can then be transduced without requiring the strong measurement associated with other means to surpass the SQL, such as back-action evasion[12].

The quadrature of motion out-of-phase with the parametric drive exhibits a reduction in noise to below the thermal level[10, 13], leading to additional applications of parametric modulation[14–16]. This “squeezed” thermal distribution can, for instance, be used to mitigate the effect of other nonlinearities in a driven oscillator by reducing either phase or amplitude noise[14]. Furthermore, the noise in one quadrature can be further reduced to below the ground state variance  $V_g$ , an effect referred to here as “quantum squeezing”. This kind of nonclassical mechanical state is a precursor to tests of macro-scale entanglement and quantum gravity[17]. However, in all previous experiments the steady-state squeezed variance has been constrained to a minimum of 50% of the original variance by a well-known 3dB limit[18]. Since the initial oscillator variance is  $V_T = V_g(2N_{\text{th}} + 1)$ , where  $N_{\text{th}}$  is the mean phonon occupation from coupling to a thermal bath, this limit leads to a stringent temperature requirement of  $N_{\text{th}} < 1/2$  for steady-state quantum squeezing. For typical micro- and nano-mechanical oscillators with resonance frequencies in the range of 1-

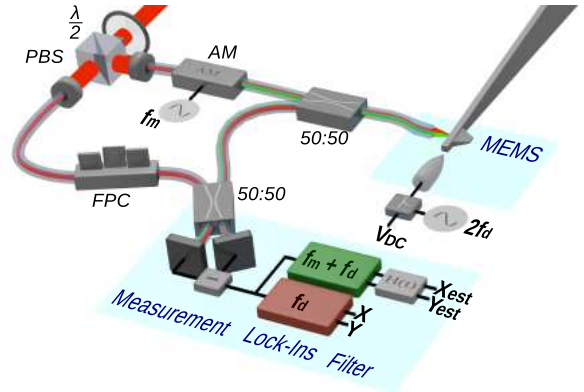


FIG. 1. Schematic of the experimental setup. The red path denotes the high-fidelity carrier signal while the green path denotes the low-fidelity signal created by amplitude modulation (AM).

100MHz, this imposes a pre-cooling temperature requirement between 0.05 and 5mK, outside the range of most conventional cryogenic setups. Here, we demonstrate squeezing below 3dB for the first time, both transient and in the steady-state. The former is achieved by operating outside of equilibrium, as demonstrated previously in ion traps[19], while conditional steady-state squeezing is demonstrated by using detuned parametric driving and optimal estimation[20]. Our results provide a path towards enhanced force sensitivity[21] as well as precise control and robust quantum squeezing of mechanical oscillators at high temperature in the absence of strong measurement[20].

The experimental setup is shown in Fig. 1. The position of a standard AFM cantilever is monitored using a Mach-Zender interferometer in a balanced homodyne configuration, with a fiber tip used to focus the optical field onto the cantilever. The cantilever resonance frequency  $f_0$  is modified from 9.6kHz to 12.5kHz upon applying a 450V potential difference between the cantilever and electrode; an effect due to the nonlin-

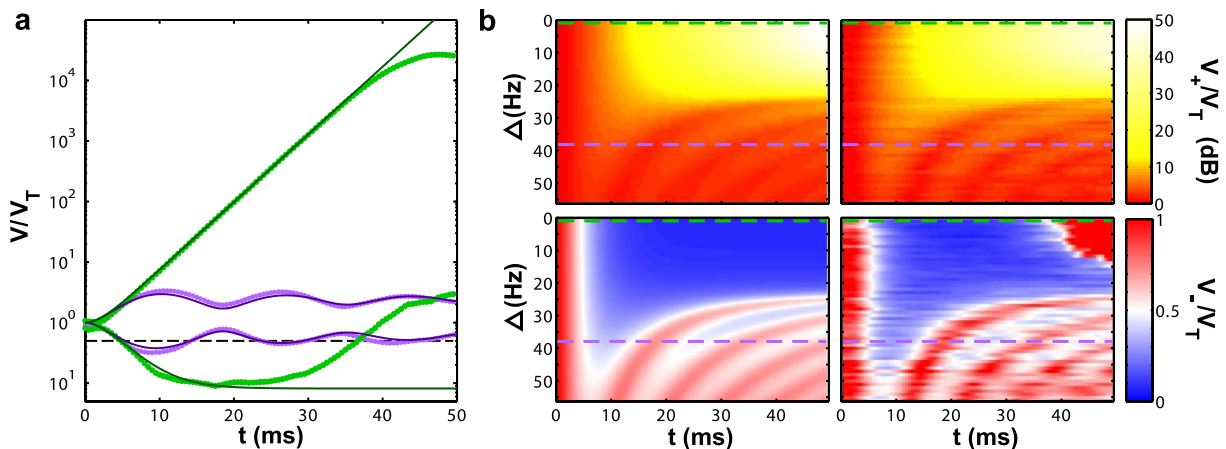


FIG. 2. Evolution of the squeezed and antisqueezed quadratures with a drive applied at  $t = 0$ . (a) Variance vs time traces for an on-resonance drive (green) and a below-threshold detuned drive (purple) for  $\chi = 22.5\text{Hz}$  with the cantilever tuned to  $f_0 = 12.5\text{kHz}$ . Solid lines are theoretical fits, while points show experimental statistics generated from 200 iterations of the drive turn-on. At each point in time, the quadratures are rotated so that the covariance  $\langle XY \rangle - \langle X \rangle \langle Y \rangle \approx 0$  over all iterations. A ring-up time of 2.5ms is chosen for the parametric drive to minimise impulse forces on the cantilever. Saturation due to the limit of fringe visibility can be seen for amplification above threshold, coinciding with a degradation of measured squeezing. (b) Theoretical (left) and experimental (right) variances as a function of detuning and time. Blue areas indicate squeezing below 3dB.

ear position dependence of capacitive energy in this geometry[7]. This large DC offset increases the peak-to-peak frequency modulation  $\chi$  for a given superimposed AC voltage[8]. A lock-in amplifier with a bandwidth much wider than the oscillator decay rate  $\gamma$  allows the dynamics to be observed in quadrature phase space, which shows the oscillation amplitude and phase with respect to a reference frequency. The orthogonal quadratures  $X$  and  $Y$  then appear as components of the position  $x = X \cos(2\pi f_d t) + Y \sin(2\pi f_d t)$  where we define an arbitrary reference frequency  $f_d = f_0 + \Delta$ . The parametric effect from an alternating voltage at frequency  $2f_d$  applied between the electrode and cantilever leads to a preferred phase of mechanical oscillation and hence a squeezed thermal distribution in the X-Y plane.

When driven on resonance ( $\Delta = 0$ ), and with a strength above the instability threshold ( $\chi > \gamma$ ), squeezing below 3dB can be achieved while the orthogonal quadrature is amplified indefinitely. Figure 2a shows the time-evolution of the maximally squeezed and antisqueezed quadrature variances measured in this regime, with  $\chi = 22.5\text{Hz}$  and  $\gamma = 2\text{Hz}$ . Good agreement with theory is observed at short times ( $< 20\text{ms}$ ) with exponential growth of the amplified quadrature and classical squeezing approaching 11dB in the orthogonal quadrature. However, the amplified quadrature saturates after approximately 35ms, where the amplitude approaches the optical quarter-wavelength of 195nm and oscillations are no longer confined to the linear portion of the interference fringe. Crucially, a side-effect of this measurement nonlinearity is a severe degradation in observed squeezing well before saturation is apparent. Such limits to

dynamic range therefore preclude the generation of all but transient squeezing above threshold. Nonetheless the strong squeezing observed reproduces the nonequilibrium squeezing observed in trapped ions[19] for the first time in a micromechanical oscillator, albeit in the classical regime.

By detuning the parametric drive off resonance, the oscillator phase undergoes a net rotation with respect to the amplification axis, increasing the instability threshold to  $\chi_{th} = \sqrt{\Delta^2 + \gamma^2}$ [20]. Consequently for the drive strength used here ( $\chi = 22.5\text{Hz}$ ), the oscillator is unstable for detunings below  $\Delta = 22.4\text{Hz}$ . When the detuning is increased further so that  $\Delta > \chi$ , the phase-space trajectories form stable elliptical orbits, as illustrated in Fig. 3a. The variances initially mirror this oscillatory behaviour before relaxing to steady-state values in the long time limit, in quantitative agreement with theoretical modelling[18]. The effect of increasing detuning on the transient statistics can be seen in Fig. 2b, where a dramatic change from monotonic behaviour to clear oscillations in the variance occurs at the threshold detuning. Notably, instantaneous squeezing below 3dB is still possible below threshold, owing to the rapid drive turn-on. The final steady-state variances can be expressed with respect to the thermal variance  $V_T$  as  $V_{\pm}/V_T = (1 \mp \chi/\chi_{th})^{-1}$ . The squeezing limit of  $V_T/2$  is therefore — while not a constraint outside of equilibrium — a fundamental one when in the steady-state.

From the above observations, the benefit of a parametrically driven system in equilibrium would appear to be limited to enhanced readout in one quadrature and 3dB reduced variance in the other. However, these phenom-

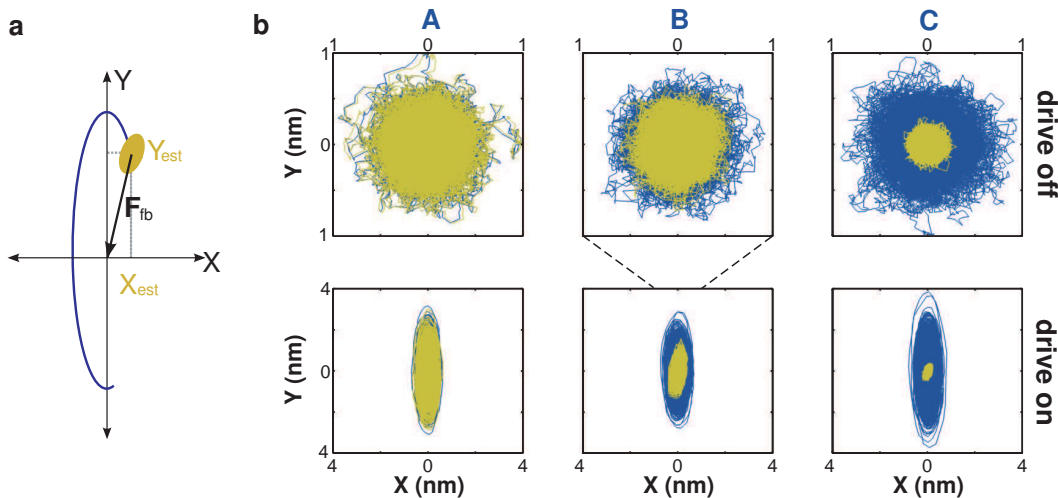


FIG. 3. Lowering conditional variance via estimation. (a) Typical phase-space trajectory over a short time with a detuned parametric drive applied to the oscillator. The estimates  $\{X_{est}, Y_{est}\}$  at a given time are calculated by filtering the low-fidelity data, and agree with a high-fidelity measurement (blue curve) to within an uncertainty (yellow ellipse). A feedback force  $F_{fb}$  can be modelled by subtracting the estimates from the high-fidelity data. (b) Quadrature phase-space trajectories for 22.5 second samples obtained from high-fidelity measurement (blue) and the residual after subtracting the estimate (yellow). The upper panels show the random-walk pattern in the undriven case mixed down at the resonance frequency  $f_0 = 14.5\text{kHz}$  for weak (A), intermediate (B) and strong measurement (C). The lower panels show the elliptical trajectories and residual noise for a parametric drive strength of  $\chi = 57\text{Hz}$  detuned close to threshold and using the same SNR as above.

ena can be combined using detuning for precise position estimation[18]. For an oscillator that is detuned so that  $\Delta > \chi$  and has relaxed to the steady-state, the thermally excited oscillations will alternate between amplified and squeezed quadratures before decaying. Since the dynamics of the system are well known, a measurement of the amplified quadrature will provide some capacity to estimate the squeezed quadrature at a later time. The squeezed quadrature therefore obtains an effective sensitivity enhancement without amplifying its mechanical fluctuations.

Using control theory, the filter that extracts the best quadrature estimates from noisy data can be written in terms of parameters defining the oscillator's expected time-evolution along with the measurement sensitivity[18]. The effective precision of these estimates can then be quantified using conditional variances. For example, the conditional variance of the  $X$  quadrature is defined as  $V_X = \langle (X(t) - X_{est}(t))^2 \rangle$  where  $X_{est}(t)$  is the best estimate available from all prior measurement results at time  $t$ . This quantity equals the unconditional variance  $\langle X^2 \rangle$  in the weak measurement limit, and is quantum-limited to the mechanical ground-state variance for an ideal continuous measurement without parametric driving[11]. The conditional variance also defines the minimum effective temperature of a quadrature achievable from ideal feedback cooling, equivalent to applying phase-space displacements in the  $X$  and  $Y$  quadratures by  $X_{est}$  and  $Y_{est}$  respectively over time.

In order to verify that the expected filter parameters

produce the best possible estimate and quantify the resulting conditional variance, we use a bright optical field to provide a high-fidelity measurement of  $X$  and  $Y$ . As shown in Fig. 1, a weak sideband is created using an intensity modulation of the bright field in order to provide low-fidelity measurements  $\tilde{X}$  and  $\tilde{Y}$  with independent shot-noise characteristics. The estimates are obtained from  $\tilde{X}$  and  $\tilde{Y}$  in post-processing and compared to the high-fidelity measurements  $X$  and  $Y$ . This use of two independent measurements to calculate the conditional variance is depicted in Fig. 3a.

The strength of the low-fidelity measurement can be naturally expressed in terms of a signal-to-noise ratio (SNR), quantified here as the ratio of mean-square thermal displacement to the square of the minimum distance resolvable over a time  $\Delta t \approx 1/4\gamma$ [22]. The SNR was set by varying the modulation depth and thus the sideband intensity. The two continuous measurements of the cantilever motion were then recorded in both the undriven case and using a parametric drive  $\chi = 57\text{Hz}$ , with a detuning of  $\Delta = 63\text{Hz}$  to ensure the below-threshold condition. Optimal  $X$  and  $Y$  estimates were then generated in post-processing by minimising the respective conditional variances over the filter parameters.

For an undriven oscillator, the optimal filter is of the form  $X_{est}(t) = g_0 \tilde{X}(t) * e^{-\Gamma_0 t}$  and  $Y_{est}(t) = g_0 \tilde{Y}(t) * e^{-\Gamma_0 t}$ . In this case, the conditional variances should be equal, i.e.  $V_X = V_Y = V_0$  and their reduction from the thermal variance  $V_T$  is a function of the measurement strength. Phase-space Brownian trajectories  $\{X, Y\}$ , de-

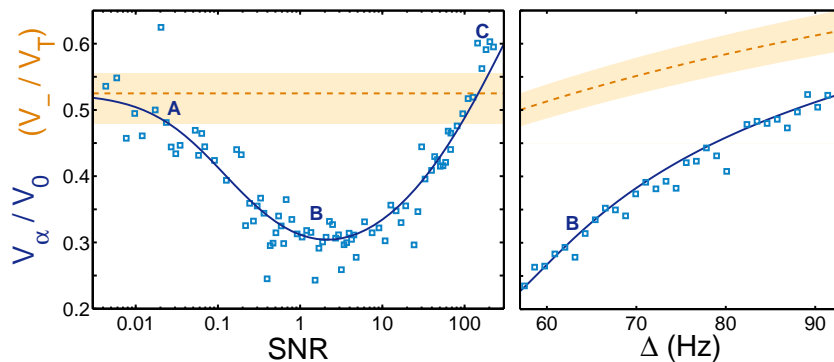


FIG. 4. Steady-state conditional squeezing. Squeezing ratios are plotted against SNR for  $\Delta = 63\text{Hz}$  (left) and against detuning for  $\text{SNR} \approx 1$  (right). Blue points show the conditional squeezing ratio, with theoretical fits shown as solid lines. Dotted red curves are fits to the unconditional squeezing, limited to  $1/2$ , with shaded bands to represent the experimental error margin. Labels A-C indicate the datapoints used to generate the trajectories in Figure 3.

terminated from the high-fidelity measurement, and corresponding residual noise  $\{X - X_{est}, Y - Y_{est}\}$  after applying this optimised filter are plotted in Fig. 3b for weak, intermediate and strong measurements. As the thermal signal increases towards the noise floor (SNR approaches 1) the optimal filter bandwidth  $\Gamma_0 = \gamma(1 + 4\text{SNR})$  begins to widen and the conditional variances drop sharply as expected. At maximum sideband intensity, the RMS uncertainty is reduced from the thermal value of 240pm to a conditional value of 60pm.

With a detuned parametric drive turned on, the two quadratures are no longer independent and the estimates require a more complex convolution

$$\begin{bmatrix} X_{est} \\ Y_{est} \end{bmatrix} = \mathbf{H}(t) * \begin{bmatrix} \tilde{X}(t) \\ \tilde{Y}(t) \end{bmatrix}, \quad (1)$$

where for  $\chi < \Delta$ , the optimal filter matrix  $\mathbf{H}(t)$  takes the general form[18]

$$\mathbf{H}(t) = \begin{bmatrix} g_1 \cos(\Omega t - \phi) & g_2 \sin(\Omega t) \\ g_3 \sin(\Omega t) & g_4 \cos(\Omega t + \phi) \end{bmatrix} e^{-\Gamma t}. \quad (2)$$

Here  $g_n$ ,  $\Omega$ , and  $\phi$  are positive real numbers. These parameters, as well as the angle  $\alpha$  of the maximally squeezed quadrature, are functions of SNR, drive strength and detuning. As in the undriven case, the squeezed variance  $V_\alpha$  is obtained by optimising over all filter parameters and the squeezing angle  $\alpha$ .

The squeezing ratio  $V_\alpha/V_0$  determined from this analysis is shown in Fig. 4 as a function of SNR and agrees well with theory. The obtained filter parameters are close to those derived from theory[18], as shown in the Supplementary Information. As expected, the variances reproduce the unconditional squeezing in the weak measurement limit and the parametric drive has no effect in the strong measurement limit. However, in the intermediate regime where  $\text{SNR} \approx 1$  there is a distinct minimum of  $V_\alpha/V_0 \approx 0.3$ , breaking the 3dB limit by a significant factor. As can be seen in Fig. 4 (right), the squeezing can be

improved further by adjusting detuning closer to threshold. These results can be understood by the fact that the effective increased sensitivity due to the parametric drive is of greatest benefit near the noise floor and with maximal amplification of the orthogonal quadrature. Since the maximum squeezing is proportional to  $\sqrt{\chi/\gamma}$ , it can be enhanced by increasing the parametric drive strength. In principle, this squeezing can be made arbitrarily large, subject to the condition  $\chi \ll f_0$ . Since the required filter (Eq. 2) can be integrated into a feedback loop, this allows arbitrary suppression of one quadrature of motion, circumventing the usual constraint associated with the measurement precision.

Although demonstrated with thermal fluctuations, our technique applies in the same manner to the zero-point motion of an oscillator, with the maximum reduction in conditional variance  $V_\alpha/V_0$  independent of temperature[18]. The action of the quantum modification at low temperatures—known as backaction noise—is instead to limit  $V_0$  to be no lower than the ground state variance. Therefore our approach could enable strong conditional quantum squeezing and, with the application of feedback, the same level of unconditional squeezing[23]. Experiments with sensitivity near the standard quantum limit (where  $\text{SNR} \approx 1$  at zero temperature) have been recently performed in mechanical oscillators[24, 25]. While purely measurement-based schemes exist to create mechanical squeezed states[12, 26], significant squeezing requires high measurement strength and efficiency such that  $\text{SNR} \gg (2N_{th} + 1)^2$ . This regime is yet to be demonstrated in mechanical oscillators. Nanoelectromechanical systems are, however, commonly integrated with a parametric drive and can be pre-cooled to near the ground state[27]. Such emerging systems are therefore good candidates for quantum squeezing below the zero-point motion using our technique, even without significant advances in transduction.

We have observed parametric squeezing of a microme-

chanical oscillator exceeding 3dB for the first time, both transient and in equilibrium, with the latter breaking a well-known limit for parametrically driven systems. This demonstrates that the 3dB limit to steady-state parametric squeezing is not fundamental, and facilitates the wider use of thermomechanical squeezing in numerous applications such as ultra-sensitive local force detection, stabilisation and precision control. The combination of parametric driving, measurement and estimation sheds light on the important interface between quantum measurement and control that is being approached most notably in opto- and electromechanical systems. The techniques introduced, if applied to state-of-the-art readout techniques and high quality oscillators, also open the door towards engineering of nonclassical states of mesoscopic mechanical systems. More broadly, these results demonstrate that combining nonlinearity with control can both overcome fundamental limitations on nonlinear processes, as well as localise mechanical motion beyond constraints imposed by the measurement sensitivity.

This research was funded by the Australian Research Council Centre of Excellence CE110001013 and Discovery Project DP0987146.

---

\* wbowen@physics.uq.edu.au

- [1] C. L. Degen, M. Poggio, H. J. Mamin, and D. Rugar, *Phys. Rev. Lett.* **100**, 137601 (2008).
- [2] P. Verlot, A. Tavernarakis, C. Molinelli, A. Kuhn, T. Antoni, S. Gras, T. Briant, P.-F. Cohadon, A. Heidmann, L. Pinard, C. Michel, R. Flaminio, M. Bahriz, O. L. Traon, I. Abram, A. Beveratos, R. Braive, I. Sagnes, and I. Robert-Philip, *Comptes Rendus Physique* **12**, 826 (2011).
- [3] S. C. Masmanidis, R. B. Karabalin, I. De Vlaminck, G. Borghs, M. R. Freeman, and M. L. Roukes, *Science* **317**, 780 (2007).
- [4] D. R. Koenig, E. M. Weig, and J. P. Kotthaus, *Nat Nano* **3**, 482 (2008).
- [5] A. D. O'Connell, M. Hofheinz, M. Ansmann, R. C. Bialczak, M. Lenander, E. Lucero, M. Neeley, D. Sank, H. Wang, M. Weides, J. Wenner, J. M. Martinis, and A. N. Cleland, *Nature* **464**, 697 (2010).
- [6] J. D. Teufel, T. Donner, D. Li, J. W. Harlow, M. S. Allman, K. Cicak, A. J. Sirois, J. D. Whittaker, K. W. Lehnert, and R. W. Simmonds, *Nature* **475**, 359 (2011).
- [7] D. Rugar and P. Grütter, *Phys. Rev. Lett.* **67**, 699 (1991).
- [8] Q. P. Unterreithmeier, E. M. Weig, and J. P. Kotthaus, *Nature* **458**, 1001 (2009).
- [9] I. Mahboob and H. Yamaguchi, *Nature Nano.* **3**, 275 (2008).
- [10] J. Suh, M. D. LaHaye, P. M. Echternach, K. C. Schwab, and M. L. Roukes, *Nano Lett.* **10**, 3990 (2010).
- [11] C. M. Caves, K. S. Thorne, R. W. P. Drever, V. D. Sandberg, and M. Zimmermann, *Rev. Mod. Phys.* **52**, 341 (1980).
- [12] A. A. Clerk, F. Marquardt, and K. Jacobs, *New J. Phys.* **10**, 095010 (2008).
- [13] R. Almog, S. Zaitsev, O. Shtempluck, and E. Buks, *Phys. Rev. Lett.* **98**, 078103 (2007).
- [14] V. Natarajan, F. DiFilippo, and D. E. Pritchard, *Phys. Rev. Lett.* **74**, 2855 (1995).
- [15] K. L. Ekinci and M. L. Roukes, *Review of Scientific Instruments* **76**, 061101 (2005).
- [16] S. Liang, D. Medich, D. M. Czajkowsky, S. Sheng, J.-Y. Yuan, and Z. Shao, *Ultramicroscopy* **84**, 119 (2000).
- [17] M. Blencowe, *Phys. Rep.* **395**, 159 (2004).
- [18] A. Szorkovszky, A. Doherty, G. Harris, and W. Bowen, *New J. Phys.* **14**, 095026 (2012).
- [19] D. M. Meekhof, C. Monroe, B. E. King, W. M. Itano, and D. J. Wineland, *Phys. Rev. Lett.* **76**, 1796 (1996).
- [20] A. Szorkovszky, A. C. Doherty, G. I. Harris, and W. P. Bowen, *Phys. Rev. Lett.* **107**, 213603 (2011).
- [21] D. Vitali, S. Mancini, L. Ribichini, and P. Tombesi, *Phys. Rev. A* **65**, 063803 (2002).
- [22] A. C. Doherty, A. Szorkovszky, G. Harris, and W. Bowen, *Phil. Trans. R. Soc. A* **370** (2012).
- [23] H. M. Wiseman and G. J. Milburn, *Phys. Rev.* **49**, 1350 (1994).
- [24] J. B. Hertzberg, T. Rocheleau, T. Ndukum, M. Savva, A. A. Clerk, and K. C. Schwab, *Nat. Phys.* **6**, 213 (2010).
- [25] A. Schliesser, O. Arcizet, R. Riviere, G. Anetsberger, and T. J. Kippenberg, *Nat. Phys.* **5**, 509 (2009).
- [26] M. R. Vanner, I. Pikovski, G. D. Cole, M. S. Kim, Č. Brukner, K. Hammerer, G. J. Milburn, and M. Aspelmeyer, *Proc. Nat. Acad. Sci. USA* **108**, 16182 (2011).
- [27] B. H. Schneider, S. Etaki, H. S. J. van der Zant, and G. A. Steele, *Sci. Rep* **2**, 599 (2012).

Supplementary Information: Filtering of time-series steady-state data

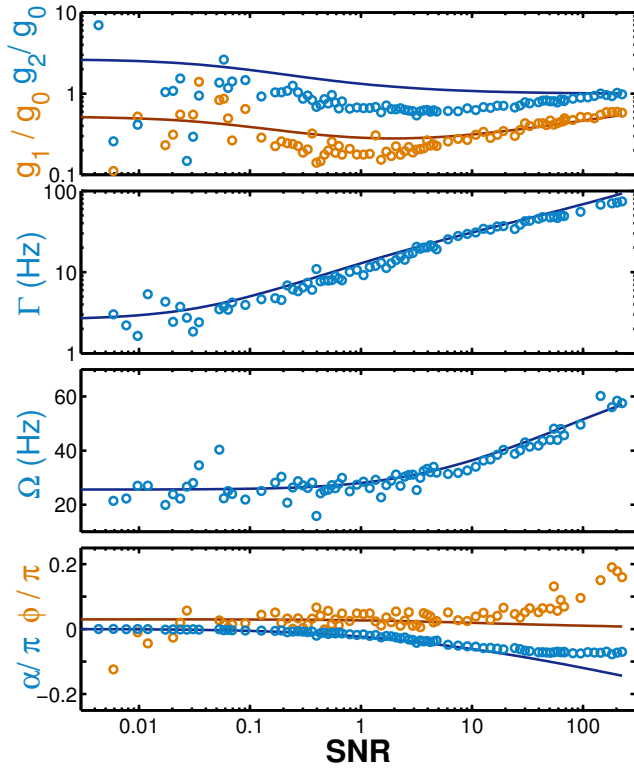


FIG. A1. Optimal filter parameters. Solid lines indicate theoretical parameters for  $\chi = 57\text{Hz}$ ,  $\gamma = 2.6\text{Hz}$  and  $\Delta = 63\text{Hz}$ . Circles indicate parameters obtained from post-processing.

At each sideband intensity featured in Fig. 4, simulta-

neous 45-second traces of the lock-in outputs  $X, Y, \tilde{X}, \tilde{Y}$  were recorded using a data acquisition unit with no parametric drive applied to the cantilever. Throughout the experiment, during these thermal measurements the oscillator resonance  $f_0$  was kept within 5Hz of the lock-in reference frequency. Data acquisition was then repeated using parametric drives of various detunings at the same sideband intensity. The lock-in reference frequency — now shifted by  $\Delta$  — is kept phase-locked to the drive voltage. A lock-in time constant of  $\tau_c = 300\mu\text{s}$  was used so that the output oscillations (limited in frequency to  $\Delta$ ) are contained within the output bandwidth.

In post-processing, the conditional variance  $V_X$  was found by convolving the time series with a filter function (truncated to 22.5 seconds) and calculating  $\langle (X - X_{est})^2 \rangle$  over the second half of the data. In the thermal case, the filter is characterised by a gain  $g_0$ , a decay rate  $\Gamma_0$  and a small rotation frequency  $\Omega_0$  to account for drifts in  $f_0$ . The optimum conditional variance was then found by minimising computationally over all filter parameters.

In the parametrically driven case, the measurement quadratures were initially rotated to be aligned with the unconditional squeezing. Optimal estimates of the filter parameters were then calculated based on known quantities: thermal signal-to-shot noise level (SNR), decay rate  $\gamma$ , drive strength  $\chi$  and detuning  $\Delta$ [18]. These initial parameters are shown as solid lines in Fig. A1 for the dataset analysed in this paper. Since the conditional squeezing angle is a function of SNR and other parameters, a quadrature rotation  $\alpha$  is included among the parameters. The obtained optimal filter agrees reasonably well with theoretical estimates, although more likely to converge to consistent values in the higher-fidelity regime and in regions with more distinct minima. This demonstrates that the optimal filter parameters described in Ref. [18] agree quantitatively with experiment.